Pergamon

Scripta Materialia, Vol. 40, No. 7, pp. 859–872, 1999
Elsevier Science Ltd

1359-6462/99/$–see front matter

PII S1359-6462(99)00041-X

EXPERIMENTALLY-BASED MICROMECHANICAL MODELING OF DYNAMIC RESPONSE OF MOLYBDENUM

Sia Nemat-Nasser, Weiguo Guo and Mingqi Liu
Center of Excellence for Advanced Materials, Department of Applied Mechanics, and Engineering Sciences, University of California, San Diego, 9500 Gilman Drive, La Jolla, CA 92093-0416

(Received January 21, 1999)
(Accepted February 1, 1999)

1. Introduction

Molybdenum (Mo), a bcc metal with a melting point of 2,610°C and a density of 10.22 g/cm^3, is an important refractory metal. The refractory properties of molybdenum reflect the high strength of interatomic bonding resulting from the overlap of the 4d-orbitals and the number of bonding electrons available (1).

The melting point of molybdenum is exceeded only by those of tungsten and tantalum, among the useful high-temperature metals. This makes molybdenum essentially a "hot strength" material. Molybdenum is *ductile* at room temperature, with a brittle-ductile transition temperature significantly lower than that of tungsten. The density of molybdenum is approximately 62% of that of tantalum, and is approximately one half of that of tungsten, making molybdenum a good candidate for applications where high-temperature capability, weight considerations, and ductility are key issues.

Molybdenum also possesses much greater specific heat than either tantalum or tungsten, making it easier to thermally treat molybdenum to produce structures with low thermal stresses than most other metals. Molybdenum is resistant to most chemical reagents except for oxidizing acids. The relatively low thermal neutron cross section of molybdenum also makes it suitable for nuclear applications. The unique properties of molybdenum make it an ideal material for high-temperature engineering applications. Since the 1960's, molybdenum has also been chosen by many researchers as an ideal material to examine the deformation behavior of bcc metals. These studies have, however, focused on low strain-rate regimes.

The deformation characteristics of bcc metals differ markedly from those exhibited by fcc metals. For example:

1) the yield strength and flow stress of bcc metals increase rapidly with decreasing temperature and increasing strain rate, in contrast to the much more modest trends exhibited by fcc metals,
2) the activation volume for the deformation of bcc metals is in the range of 5–50b^3 (b = magnitude of Burgers' vector of dislocations), whereas that for fcc metals is often 10–100 times greater,
3) the increase in the yield point with a decrease in temperature is independent of the strain-hardened state in bcc metals, whereas it is greater for the higher strain-hardened states for fcc metals.

The study of the deformation behavior of molybdenum is expected to lead to a more detailed understanding of the deformation mechanisms of bcc metals, in particular the refractory metals. The

focus of the present work has been on the high strain-rate, high strain response of molybdenum, over a broad range of temperatures. Before presenting our experimental and the corresponding micromechanical modeling results, we briefly review some of the existing relevant contributions.

1.1. Existing Modeling Efforts

Like for many other bcc metals, the strength, hardening, ductility, and deformation behavior of molybdenum are strong functions of the temperature, strain, strain rate, and substructure. Steinberg (2) applied the Steinberg-Guinan-Lund rate-dependent constitutive model (3,4) to molybdenum. The hydrodynamic equation of state used in the calculation is a Mie-Gruneisen equation with a linear shock-velocity, particle-velocity relation. The model was used to simulate rate-dependent phenomena, such as shock smearing and precursors on re-shock. The model is physically-based and the parameters can be determined from non-shock-wave sources.

Tanoue and Matsuda (5) superposed stress relaxation curves for polycrystalline molybdenum, obtained from stress relaxation tests and plotted as stress vs. strain rate in log scale, and formed unique master curves. These master curves can be further superposed by scaling. It is suggested by these authors that the primary shapes of the master curves are not affected by grain size and strain rate. Furthermore, the master curves obtained by changing the amount of impurities and temperatures could not be superposed on each other because of the different shapes of the master curves. Based on an analysis of various activation parameters, the authors concluded that the rate-controlling mechanism of molybdenum during stress relaxation is the thermally activated overcoming of the Peierls-Nabarro hills by the double-kink nucleation; this is similar to that of tantalum, as discussed by Nemat-Nasser and Isaacs (6).

In order to examine the effect of alloying elements on the creep behavior of molybdenum at elevated temperatures, a semi-mechanistic model for molybdenum subjected to low strain-rate deformation is proposed by Gao and Zee (7). The authors modeled the Class II creep behavior observed in molybdenum alloys and found that an increase of solute concentration results in a change of the dominating creep mechanism from climb-controlled to glide-controlled.

1.2. Temperature Effects

Temperature has a significant impact on the deformation behavior of molybdenum. The influence of temperature on the microstructure and properties of molybdenum can be classified as: 1) the pre-deformation heat treatment temperature (annealing temperature), and 2) the deformation temperature.

Molybdenum has a recrystallization temperature of approximately 900°C. In general, its annealing temperature is between 870 and 980°C; this ensures a fully recrystallized microstructure. The maximum ductility occurs at an annealing temperature of 1,020°C. It is noted that too high an annealing temperature would result in undesirable properties. An investigation conducted by Sququet *et al*. (8) on sintered and melted molybdenum indicates that annealing of cold worked molybdenum at 1,200°C would result in intergranular fracture which is attributed to the impurity segregation at the grain boundaries.

Pavlov *et al*. (9) examined the temperature dependence of three kinds of molybdenum samples with different impurity levels over a temperature range of 20–1,000°C. The authors found that the significant temperature dependence of the yield point of molybdenum is associated with the resistance of the lattice to the dislocation motion, i.e., the Peierls stress is the dominant stress during the deformation of molybdenum at elevated temperatures.

Test results for polycrystalline molybdenum (grain size of 4–120 μm) subjected to tensile deformation over 20–1,600°C, indicate that a softening occurs around 1,200–1,300°C. A TEM/SEM study

reveals that the softening and uniform deformation of molybdenum in this temperature range are due to the rapid development of grain-boundary slip (10). A decrease in grain size greatly improves the yield point and the tensile strength at room temperature, in compliance with the Hall-Petch relation. Fine-grain molybdenum remains stronger than the large-grain material up to 1,200°C. Below $0.4T_m$, the plastic deformation is mainly achieved by subgranular slip, whereas grain-boundary sliding becomes dominant at higher temperatures.

1.3. Strain-Rate Effects

High strain-rate dependence is a common characteristic shared by many bcc metals. A study on the strain-rate effect on the deformation behavior of molybdenum was performed by Briggs and Campbell (11). In their study, polycrystalline molybdenum specimens were deformed in compression at strain rates from 10^{-4} to 10^{2}/s, over a temperature range of 77 to 600°C. It is concluded by these authors that the temperature sensitivity and rate sensitivity of the lower yield stress and of the flow stress at 8% strain are essentially constants for certain temperatures and strain rates. Therefore, flow can be described by a single thermal-activation rate equation. The free energy of activation is temperature- and stress-dependent. The molybdenum specimens are found to deform by twinning at extremely high compression stresses, regardless of temperature and strain rate. Also, it was concluded that the work-hardening rate of molybdenum is independent of the strain rate. The rate-controlling process in molybdenum is concluded to be the overcoming of the lattice friction stress (Peierls stress), consistent with the results obtained by other researchers.

The effect of shearbands on the polygonization and recrystallization of molybdenum has also been examined; Larikov *et al.* (12). The presence of shearbands in molybdenum has a positive influence on polygonization as a function of temperature. Within the shearbands, polygonization is absent in the temperature range of 600–1,000°C, and is greatly speeded up at temperatures higher than 1,000°C. The recrystallized grains contain traces of deformation distortions and are morphologically similar to the grains formed during dynamic recrystallization.

1.4. Dislocation Substructure

Most investigations reported in the literature regarding the dislocation substructure of molybdenum are focused on single crystals. This is because the loading axis and the desired slip systems can be controlled by using single-crystal specimens. The dislocation characteristics observed in single-crystal molybdenum, on the other hand, can apply to the polycrystalline molybdenum, as long as the dominant deformation mechanism is subgranular slip instead of grain-boundary glide.

Unlike tantalum and tungsten which often have only one dominant slip system family, i.e., {110}<111>, molybdenum often has two dominant slip systems (13). These are the {112}<111>-family and the {110}<111>- family. In general, crystals deform by double slip along two equivalent {110}<111> systems and four {112}<111> systems, while the slip bands follow the {112}-planes. It is found that nuclei of activated slip spread along the slip direction by planar motion of edge dislocations and propagate sideways by the motion of screw dislocations which can easily cross-slip. The average yield stress decreases with an increased volume fraction of the slip bands. At large plastic deformations, strain-hardening of the slip zone activates slip systems in the neighboring areas, resulting in the homogenization of slip and deformation throughout the entire specimen.

The presence of the {112}<111> slip systems has been confirmed by a study conducted by Yoo *et al.* (14). The deformation behavior of single-crystal molybdenum at 300K indicates that the slip system at the beginning of yield is (312)[111]. This slip system is dominant up to a strain of 0.09. Then the

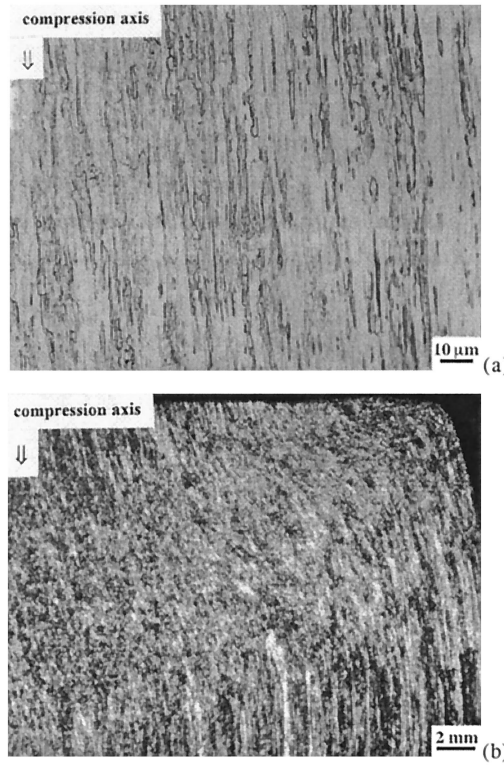

Figure 1. Microstructure of molybdenum before (a), and after testing (b).

{211}<111> slip systems become dominant. The {211}<111> slip systems are the main slip systems in molybdenum from a strain of 0.1 to a strain greater than 1.0.

A TEM study on the high-purity molybdenum single crystals deformed along the <100> and <110>-axes from 77 to 573K, reveals uniformly distributed screw dislocations when tested at temperatures below room temperature, regardless of the loading axis (15). An increase of the deformation temperature leads to the disappearance of the screw dislocations and to the formation of a cellular substructure. Both the {112}<111> and {110}<111> slip systems are observed. The resolved

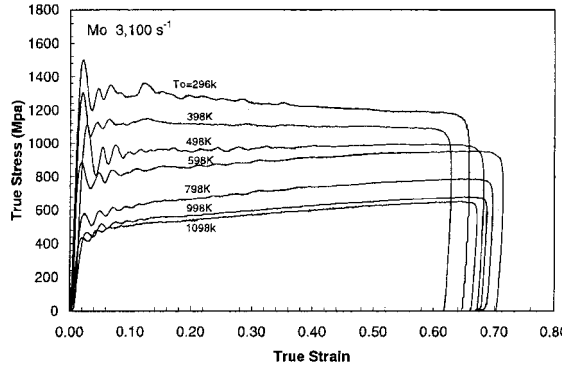

Figure 2. Adiabatic stress-strain curves at indicated initial temperatures and 3,100 s^{-1} strain rate.

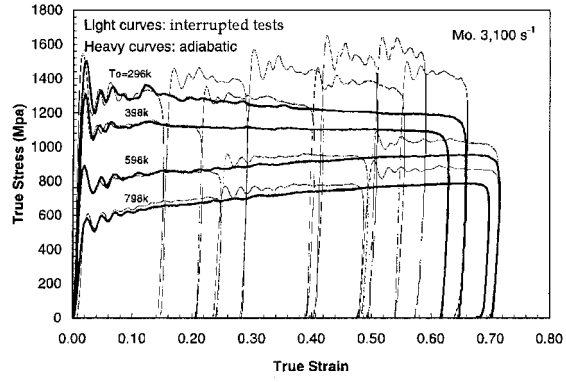

Figure 3. Interrupted tests to develop quasi-isothermal stress-strain relations for indicated initial temperatures and 3,100 s^{-1} strain rate.

shear stress of molybdenum is found to be in a linear relationship with the square root of the dislocation density.

Lau *et al*. (16) studied high-purity molybdenum single crystals oriented for the (110)[111] slip system in tension and observed that the crystals exhibit a thermally activated deformation mechanism. Based on the stress-temperature relation, activation volume vs. stress, activation volume vs. strain, the reduced kink energy, and the reduced line energy of a dislocation, the authors concluded that the Peierls mechanism is the rate-controlling deformation mechanism, with a Peierls stress estimated to be approximately 42×10^8 dyne/cm^2 at room temperature.

In-situ tensile experiments have been carried out inside a TEM on single-crystal molybdenum by Campany *et al* (17). The results obtained reveal that the operative slip systems are those having both a large Schmid factor and a small angle between the operative Burgers vector and the projection of the Burgers vector in the slip plane, i.e., slip preferentially takes place on the planes on which screw dislocations can escape easily.

1.5. Summary of Current State of the Art

A review of the literature indicates that extensive work has been performed, especially in the former Soviet Union in the 1970's, on the mechanical properties, structure, and deformation behavior of

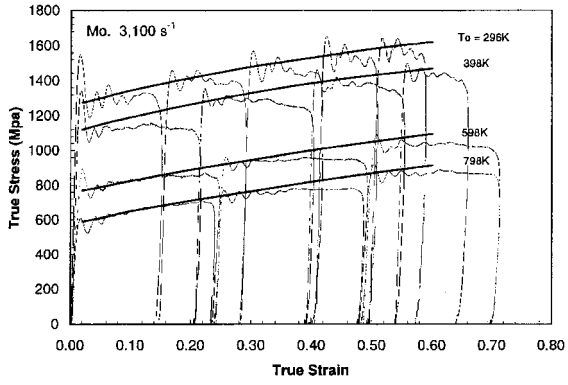

Figure 4. Quasi-isothermal stress-strain relations for indicated initial temperatures and 3,100 s^{-1} strain rate.

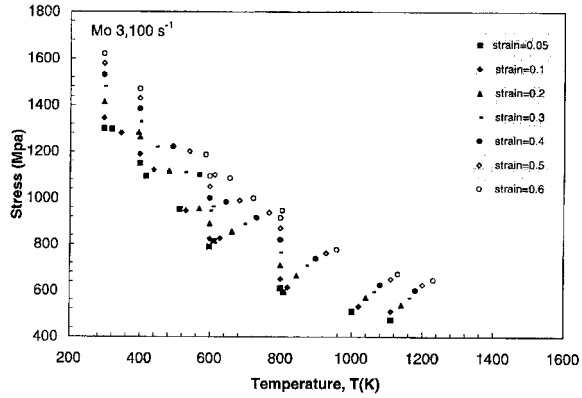

Figure 5. Flow stress as a function of temperature for indicated strain and 3,100 s^{-1} strain rate.

molybdenum, leading to certain fundamental understanding of the response of molybdenum deformed at low or moderate strain rates (10^{-4}–10^{2}/s range) (18–21). The strain rates were limited due to the limitation in the experimental instrumentation and techniques. The dynamic response of molybdenum at high and ultrahigh strain rates ($\geq 10^{3}$/s) is still unknown. Literature regarding the deformation characteristics and microstructural features of molybdenum subjected to high strain-rate compression/shear is rare or essentially nonexistent. It would be important, both fundamentally and practically, to gain knowledge in this area, in order to understand the physical and mechanical properties of molybdenum subjected to dynamic deformation, over a broad range of strain rates, strains, and temperatures. The present work is a step in this direction.

2. Experimental Procedure and Results

The material used in the present work is molybdenum of greater than 99.98% purity, received in the form of 6mm bars. Cylindrical samples of 5mm diameter and 5mm height are machined from these bars. The samples are annealed in less than a 10^{-5} mm Hg vacuum at a 900°C temperature for one hour. Some of the samples are then tested in compression, at various strain rates and temperatures. Both untested and tested samples are sectioned parallel to the compression axis and the corresponding

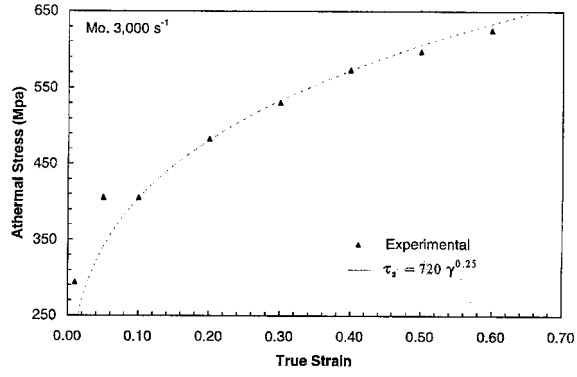

Figure 6. Limiting values of flow stress as a function of strain.

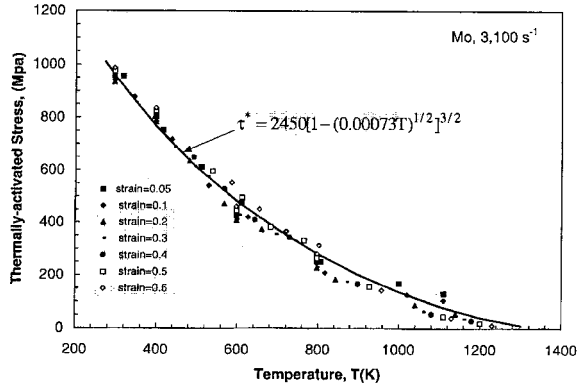

Figure 7. Thermally activated part of flow stress as a function of temperature for any strain and 3,100 s^{-1} strain rate.

microstructure is examined by optical microscopy, revealing a bamboo-type texture, as shown in Fig. 1a, which corresponds to an untested sample. The grains appear to have essentially the same <110> orientation (8,9). With this texture the material exhibits greater resistance to deformation in the axial direction than any other direction. Figure 1b shows the microstructure of a sample, after it has been axially deformed at a 3,100 s^{-1} strain rate. A shearband seems about to form at a 45° angle with the loading axis.

All high-strain-rate compression tests are performed using UCSD's recovery Hopkinson technique (6,22–24). Strains up to 70% are achieved in these tests, over a temperature range of 296–1,100K, at various strain rates. The results of a 3,100s^{-1} strain rate are used to fix the model and then the predictability of the model is checked, using the results of an 8,000s^{-1} strain rate. The details of the experimental procedure have been described elsewhere (6,24). Therefore, only the experimental results are presented here.

Figure 2 shows the adiabatic stress-strain curves for a 3,100s^{-1} strain rate and indicated initial temperatures. Figure 3 compares the adiabatic curves with the results of interrupted tests performed to obtain the corresponding quasi-isothermal stress-strain relations, for indicated temperatures. These quasi-isothermal stress-strain relations are shown in Fig. 4. As is seen, the isothermal flow stresses are essentially parallel to each other, indicating that their differences are solely due to temperature. This observation is confirmed by the results in Fig. 5, which displays the flow stress as a function of

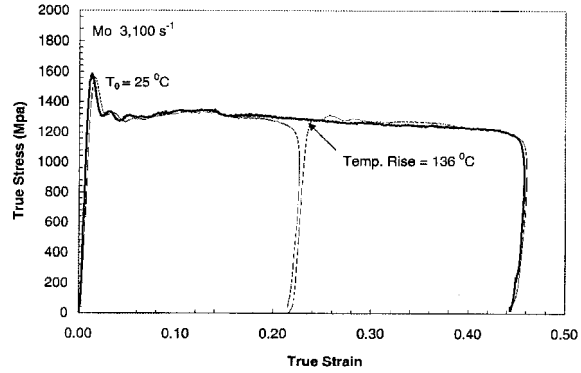

Figure 8. Verification of $\eta = 1$.

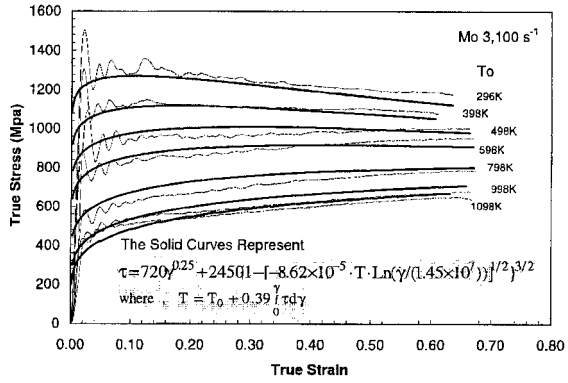

Figure 9. Comparison of model predictions with actual experimental results for indicated initial temperatures and 3,100 s^{-1} strain rate.

temperature for different strains. The data in Fig. 5 also indicate that after a critical temperature, the flow stress is essentially independent of the temperature.

3. Physically-Based Constitutive Model

As pointed out in the introduction, existing experimental observations suggest that the short-range barrier to the motion of dislocations is the lattice resistance, i. e., the Peierls stress. The results displayed in Figs. 4 and 5 are consistent with this observation. Hence, following the procedure suggested by Nemat-Nasser and Isaacs (6), we first plot the limiting values of the flow stress, obtained from Fig. 5 for the highest temperature, as a function of the strain; see Fig. 6. Then we fit this empirically with a power law,

$$\tau_a = 720\gamma^{1/4}, \tag{1}$$

and view τ_a as the athermal part of the flow stress, it being independent of the temperature, as suggested by the results in Fig. 5. We now subtract τ_a from the flow stress in Fig. 5,

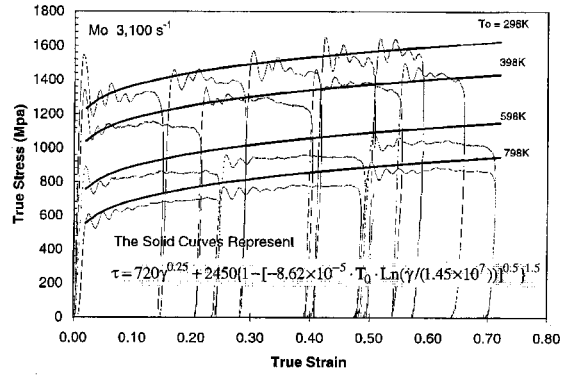

Figure 10. Isothermal predictions of Eqns. (8) compared with the results of interrupted tests for indicated initial temperatures and 3,100 s^{-1} strain rate.

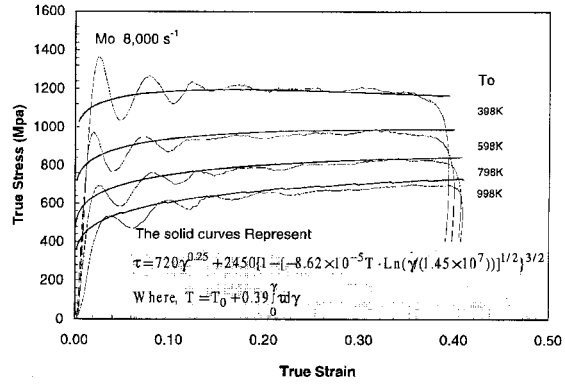

Figure 11. Verifying the predictive capability of the model: adiabatic flow stress at indicated initial temperatures and 8,000 s^{-1} strain rate.

$$\tau^* = \tau - \tau_a, \tag{2}$$

and view τ^* as the thermally activated part of the flow stress; in (2), τ is the flow stress. The resulting experimental data are now plotted in Fig. 7, and, as is seen, they collapse into essentially one curve which is shown by the solid line, having the following mathematical description:

$$\tau^* = 2{,}450[1 - (0.00073T)^{1/2}]^{3/2} \tag{3}$$

As has been suggested by Nemat-Nasser and Isaacs (6), when the resistance to the motion of dislocations consists of an athermal part τ_a, and a thermally activated one, τ^*, which is due to the Peierls resistance only, then the flow stress may be approximated, as follows:

$$\tau = \tau_a + \hat{\tau}\left\{1 - \left(-\frac{k}{G_o}T1n\frac{\dot{\gamma}}{\dot{\gamma}_r}\right)^{1/q}\right\}^{1/p}, \tag{4}$$

where $\hat{\tau}$ is the threshold stress, G_o is the total energy of the barrier, k is the Boltzmann constant, and q and p are constants defining the shape of the short-range barrier, $0 < p \leq 1$, $1 < q \leq 2$. As is indicated by the experimental results of Fig. 7 and Eqn. (3), here $q = 2$ and $p = 2/3$. These are the same values as those obtained for tantalum which is a bcc metal, whose short-range barriers correspond to the

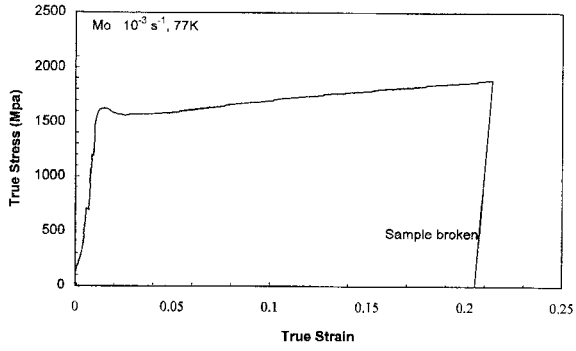

Figure 12. Stress-strain relation at 77K and 0.001 s^{-1} strain rate.

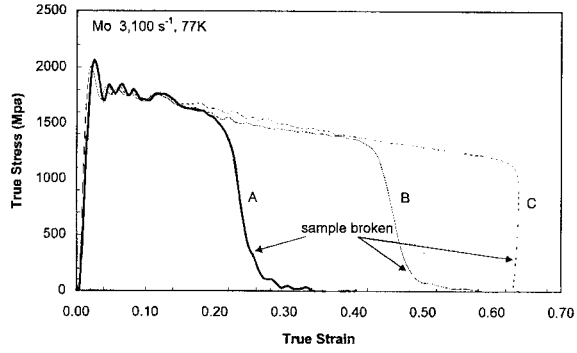

Figure 13. Stress-strain relations at 77K and 3,100 s^{-1} strain rate.

Peierls' stress, as well as for OFHC copper which is an fcc metal with forests of dislocations as its short-range barriers. In Eqn. (4), $\dot{\gamma}_r$ is the reference strain rate defined by

$$\dot{\gamma}_r = b^2 \rho_m \omega_o, \tag{5}$$

where b is the magnitude of the Burgers vector, ρ_m is the density of the mobile dislocations, and ω_O is the attempt frequency of a dislocation to overcome its short-range barrier.

From Eqn. (3) it is seen that for $T = T_c \cong 1{,}300K$, the thermally activated part of the flow stress, τ^*, is zero. This defines the critical temperature, above which the dislocations can overcome their short-range barriers, without any assistance from the thermal activation.

Comparing the general expression (4), with the specific results (3), it follows that, in this particular case,

$$-\frac{k}{G_o} 1n \frac{\dot{\gamma}}{\dot{\gamma}_r} = 0.00073. \tag{6}$$

Since $\dot{\gamma} = 3{,}100 s^{-1}$, to obtain the values of G_o and $\dot{\gamma}_r$ from (6), it is necessary to estimate $\dot{\gamma}_r$ or have a measured value for G_o. If we take G_o to be about 1eV/atom, then we can use the experimental results to fine-tune the values of k/G_o and $\dot{\gamma}_r$; the same value of G_o has been used by Nemat-Nasser and Isaacs (6) for tantalum. This procedure leads to

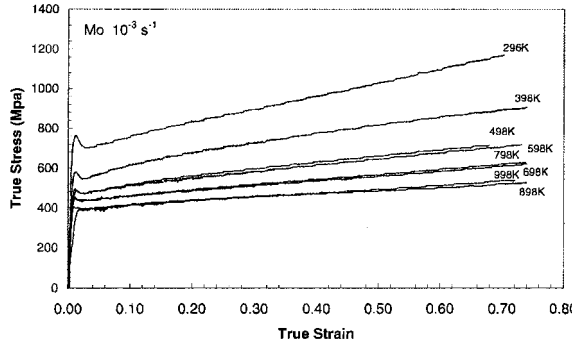

Figure 14. Adiabatic flow stress at indicated initial temperatures and 0.001 s^{-1} strain rate.

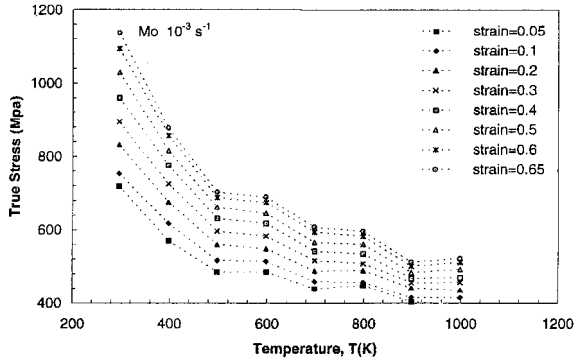

Figure 15. Flow stress as a function of temperature for indicated strain and 0.001 s^{-1} strain rate.

$$\frac{k}{G_o} = 8.62 \times 10^{-5}K^{-1}, \dot{\gamma}_r = 1.45 \times 10^{7}s^{-1}. \tag{7}$$

Now, combining all the above results, the final constitutive relations for this molybdenum become

$$\tau = 720\gamma^{1/4} + 2{,}450\left\{1 - \left[- 8.62 \times 10^{-5}T \ln\left(\frac{\dot{\gamma}}{1.45 \times 10^{7}}\right)\right]^{1/2}\right\}^{3/2},$$

$$T = T_o + \Delta T, \Delta T = \frac{\eta}{\rho C_v}\int_0^{\gamma} \tau d\gamma, \tag{8}$$

where T_o is the initial temperature, ρ is the mass density (10.22 g/cm^3), C_v is the heat capacity which varies with the temperature, and η is the fraction of the plastic work which is converted into heat. The value of η must be established based on experimental results. Data reported by Kapoor and Nemat-Nasser (25) for several metals suggest that, for large strains, e. g., $\gamma \geq 0.2$, η is essentially 1. To verify this for the present case, three tests at 3,100s^{-1} and initial temperature of $T_o = 296K$ were performed and the results are shown in Fig. 8. The first test is an adiabatic experiment to a strain of about 0.45. Then a second sample is strained to a strain of $\gamma = 0.22$ at the same initial temperature and the same strain rate. If it is assumed that the entire plastic work, for this last test, has been converted to heating

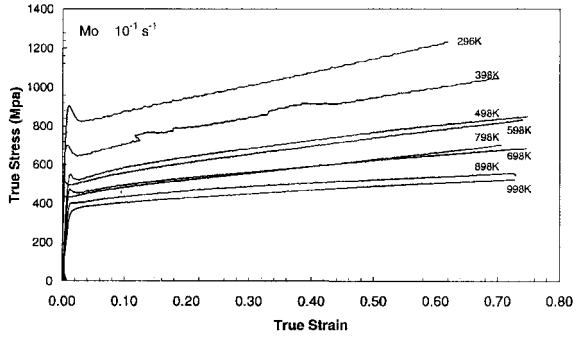

Figure 16. Adiabatic flow stress at indicated initial temperatures and 0.1 s^{-1} strain rate.

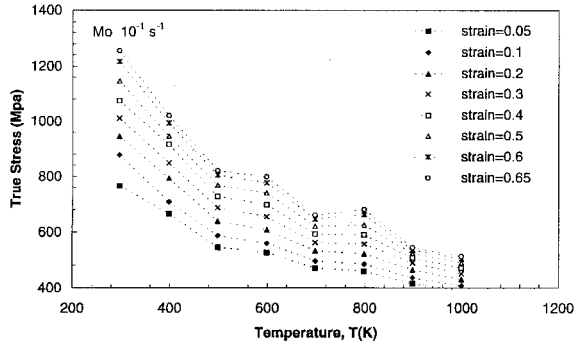

Figure 17. Flow stress as a function of temperature for indicated strain and 0.1 s^{-1} strain rate.

the sample, then a temperature increase of 136K would be achieved by the sample, at the end of this second test. If this assumption is correct, then once this second sample is cooled to a temperature of 296K, is heated to 432K, and is tested at a strain rate of 3,100s^{-1}, it should follow the adiabatic curve obtained for the first sample. Figure 8 shows that this indeed is the case. For large strains, therefore, we assume $\eta = 1$. It should be noted, however, that, if an annealed sample is strained by 1 or 2%, some (very small) part of the plastic strain would be stored as elastic energy of the dislocations. For large strains, this stored elastic energy is less than the generally expected experimental error. It can thus be ignored.

With $\eta = 1$, and using the room-temperature value of $C_v \cong 0.25$J/gK, we obtain $\eta/\rho C_v \cong 0.39$. Figure 9 compares the results obtained from Eqns. (8) with the experimental results for indicated initial temperatures. In Fig. 10 the isothermal predictions of Eqns. (8) are compared with the corresponding interrupted experimental results for indicated temperatures. To verify the predictive capability of the model, new tests at an 8,000s^{-1} strain rate are performed at various initial temperatures, as given in Fig. 11. The model results are also shown in this figure, revealing good correlation with experimental data.

4. Low-Temperature Response

We have also examined the compressive response of the material at liquid nitrogen temperature (77k) and both high (3,100s^{-1}) and low (10^{-3} s^{-1}) strain rates. The results are shown in Figs. 12 and 13. At both strain rates, the sample failed by axial fracturing, indicating a brittle response at such a low

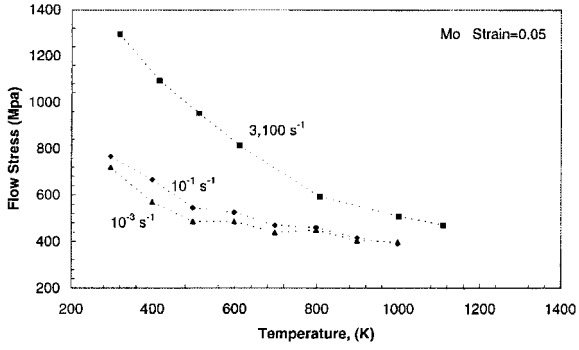

Figure 18. Flow stress as a function of temperature for indicated strain rates and 0.05 strain.

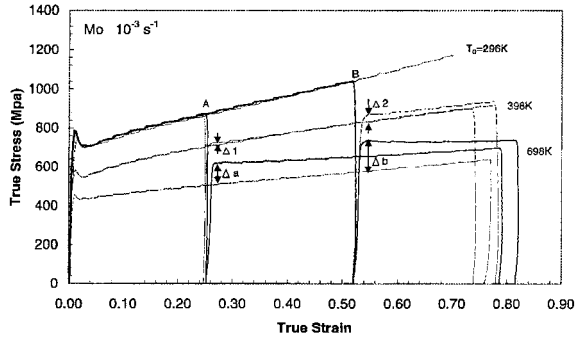

Figure 19. Isothermal predictions of Eqns. (8) compared with the results of interrupted tests for indicated initial temperatures and 0.001 s^{-1} strain rate.

temperature. At the high strain rate of 3,100 s^{-1}, the sample begins to crack axially soon upon loading, whereas at the low strain rate of 10^{-3} s^{-1}, cracking begins after 5 to 10% strain. Note the pronounced workhardening displayed by the sample for the 10^{-3} s^{-1} strain rate, even close to the failure strain.

5. Low Strain-Rate High-Temperature Response

The experimental results for a 10^{-3} s^{-1} strain rate and indicated temperatures, are given in Figs. 14 and 15. These data clearly display the presence of dynamic strain aging, occurring at two different temperatures, presumably being associated with solute atoms of two different activation energies. Similar results are obtained at a strain rate of 10^{-3} s^{-1}; see Figures 16 and 17. To compare with the high strain-rate data, we have presented in Figure 18 the flow stress of this molybdenum as a function of the temperature, for the three strain rates and a strain of 5%. As is seen, there are no dynamic strain-aging effects at the 3,100s^{-1} strain rate. Furthermore, the response at low strain rates becomes essentially temperature-independent at temperatures exceeding 900 to 1000K.

To explore the low strain-rate behavior of this molybdenum, we have performed interrupted tests at three different temperatures, as shown in Fig. 19, for a 10^{-3} s^{-1} strain rate. The light curves in this figure denote the results for three different tests, each at the indicated temperature, i.e., at T_o = 296, 398, and 698K, respectively. Then two other samples are first loaded to about 25% true strain (Point A), at a room temperature of 296K. One sample is then heated to a temperature of 398K, and the other sample to 698K, before loading them at the same strain rate of 10^{-3} s^{-1}. As is seen, the reloading at a temperature of 698K produced a yield stress greater than that which is attained by a virgin sample which is deformed continuously from zero strain, at the same temperature. For the interrupted test with the temperature jump form 296K to 398K, on the other hand, no noticeable difference in the yield stress is observed at a 25% true strain.

Similar tests are performed at a 10^{-3} s^{-1} strain rate, but with the temperature jump being introduced at a 52% true strain; Point B. A significant increase (153MPa) in the yield stress is observed when the temperature is *increased* from 296K to 698K. The corresponding increase for a jump from 296K to 398K is about 38MPa.

The model of Section 3 does not include the effects of dynamic strain aging. The authors and coworkers are now modifying this model to include the strain-aging effects at high strain rates and temperatures. Initial application of the results to predict the high strain-rate response of commercially

pure titanium over a broad range of temperatures, has been successful. Application to low strain-rate regimes of bcc materials is currently being explored.

Acknowledgment

This work has been supported by the Center of Excellence for Advanced Materials (CEAM) of University of California, San Diego.

References

1. E. R. Braithwaite and J. Haber, Molybdenum: An Outline of Its Chemistry and Uses, Elsevier, New York (1994).
2. D. J. Steinberg, J. Appl. Phys. 74, 3827 (1993).
3. D. J. Steinberg, S. G. Cochran, and M. W. Guinan, J. Appl. Phys. 51, 1498 (1980).
4. D. J. Steinberg and C. M. Lund, J. Appl. Phys. 65, 1528 (1989).
5. K. Tanoue and H. Matsuda, Trans. Jpn. Inst. Metals 25(2), 89–95 (1984).
6. S. Nemat-Nasser and J. B. Isaacs, Acta Mater. 45, 907 (1997).
7. H. Gao and R. Zee, Scripta Metall. Mater. 32, 1665 (1995).
8. S. Sququet, C. Gerard, and J. P. Traverse, J. Mater. Sci. Lett. 14, 305 (1995).
9. V. A. Pavlov, I. A. Pereturina, L. M. Postnov, S. F. Burlakov, and A. P. Tribulkin, Fiz. Metal. Metalloved. 31, 849 (1971).
10. G. A. Avtonomov, O. V. Bakun, L. S. Igolkina, V. K. Sulzhenko, and S. A. Firstov, Fiz. Metal. Metalloved. 44, 633 (1977).
11. T. L. Briggs and J. D. Campbell, Acta Metall. 20, 711 (1972).
12. L. N. Larikov, M. N. Belyakova, Y. A. Maksimenko, and P. V. Mudruk, Fiz. Metal. Metalloved. 58, 136 (1981).
13. A. Luft and C. Ritschel, Phys. Stat. Sol. 72, 225 (1982).
14. M. K. Yoo, Y. Hiraoka, and J. Choi, Scripta Metall. Mater. 33, 1461 (1995).
15. C. V. Kopetskii and A. I. Pashkovskii, Phys. Stat. Sol. 21, 741 (1974).
16. S. S. Lau, S. Ranji, A. K. Mukherjee, G. Thomas, and J. E. Dorn, Acta Metall. 15, 237 (1967).
17. R. G. Campany, R. E. Smallman, and M. H. Loretto, Mater. Sci. No. 8, 261 (1976).
18. Y. M. Vitorskiy, R. K. Ivaschenko, S. N. Kaverina, D. V. Lotsko, Y. V. Milman, and V. I. Trefilov, Fiz. Metal. Metalloved. 35, 1064 (1973).
19. Y. M. Vitorskiy, Y. Y. Zubets, S. N. Kaverina, V. A. Manilov, V. I. Trefilov, and S. A. Firstov, Fiz. Metal. Metalloved. 33, 831 (1972).
20. A. N. Vergazov, V. A. Likhachev, and V. V. Rybin, Fiz. Metal. Metalloved. 42, 1241 (1976).
21. A. D. Vasilyev, I. S. Malashenko, V. I. Trefilov, S. A. Firstov, and O. P. Shigonova, Fiz. Metal. Metalloved. 43, 640 (1977).
22. S. Nemat-Nasser, J. B. Isaacs, and J. E. Starrett, Proc. R. Soc. 435A, 371 (1991).
23. S. Nemat-Nasser, Y. F. Li, and J. B. Isaacs, Mech. Mater. 17, 111 (1994).
24. S. Nemat-Nasser and Y. L. Li, Acta Mater. 46, 565 (1998).
25. R. Kapoor and S. Nemat-Nasser, Mech. Mater. 27, 1 (1998).